

Ferrobustamite: The crystal structures of two Ca,Fe bustamite-type pyroxenoids*

By PHILIP A. RAPOPORT and CHARLES W. BURNHAM

Department of Geological Sciences, Harvard University

(Received 7 March 1973)

Auszug

Die Strukturen zweier pyroxenartiger Kristalle, eines synthetischen, $\text{Ca}_{1/2}\text{Fe}_{1/2}\text{SiO}_3$, und eines natürlichen von etwa der Zusammensetzung $\text{Ca}_{0,79}\text{Fe}_{0,19}\text{Mn}_{0,02}\text{SiO}_3$, wurden mittels der Methode der kleinsten Quadrate und aus den an Einzelkristallen mit einem automatischen Diffraktometer gemessenen Intensitäten verfeinert. Die Raumgruppe ist in beiden Fällen $A\bar{1}$; die Gitterkonstanten sind: $a = 7,69 \text{ \AA}$, $b = 7,11 \text{ \AA}$, $c = 13,765 \text{ \AA}$, $\alpha = 90^\circ 22'$, $\beta = 95^\circ 19'$, $\gamma = 103^\circ 58'$ bzw. $a = 7,83 \text{ \AA}$, $b = 7,23 \text{ \AA}$, $c = 13,925 \text{ \AA}$, $\alpha = 90^\circ 1'$, $\beta = 95^\circ 24'$, $\gamma = 103^\circ 21'$. Im synthetischen Kristall sind Fe und Ca auf zwei allgemeine und zwei spezielle Lagen geordnet verteilt. Obwohl die genaue Verteilung der Kationen im natürlichen Kristall sich wegen dessen Verzwilligung nicht sicher bestimmen ließ, gibt es doch starke Anhaltspunkte dafür, daß die meisten Fe- und Mn-Atome in *einer* speziellen Lage angeordnet sind. Kristallechemische Betrachtungen bestätigen die vermutete Grenze, bis zu welcher Eisen vom Bustamit aufgenommen werden kann.

Abstract

The crystal structures of two pyroxenoids having compositions $\text{Ca}_{0,5}\text{Fe}_{0,5}\text{SiO}_3$ and approximately $\text{Ca}_{0,79}\text{Fe}_{0,19}\text{Mn}_{0,02}\text{SiO}_3$ have been refined using least-squares techniques from single-crystal x-ray intensity data measured with an automated diffractometer. Both pyroxenoids have approximately the same unit-cell parameters and structures as bustamite: Space group $A\bar{1}$; $a = 7.69 \text{ \AA}$, $b = 7.11 \text{ \AA}$, $c = 13.765 \text{ \AA}$, $\alpha = 90^\circ 22'$, $\beta = 95^\circ 19'$, $\gamma = 103^\circ 58'$; and $a = 7.83 \text{ \AA}$, $b = 7.23 \text{ \AA}$, $c = 13.925 \text{ \AA}$, $\alpha = 90^\circ 1'$, $\beta = 95^\circ 24'$, $\gamma = 103^\circ 21'$ respectively. The synthetic crystal of $\text{Ca}_{0,5}\text{Fe}_{0,5}\text{SiO}_3$ has Fe and Ca ordered over two general and two special positions. Although twinning prevented an accurate determination of the cation distribution in the natural crystal of $\text{Ca}_{0,79}\text{Fe}_{0,19}\text{Mn}_{0,02}\text{SiO}_3$, there

* Dedicated to Professor M. J. Buerger on occasion of his 70th birthday.

are strong indications that most of the Fe and Mn are ordered in one special position. From crystal-chemical considerations the likely composition limits of ferrobustamite can be ascertained.

Introduction

As early as the 1930's, BOWEN, SCHAIRER, and POSNJAK (1933) identified a high-temperature Ca,Fe pyroxenoid phase in the CaO—FeO—SiO₂ ternary system which they called "wollastonite solid solution". They claimed to be able to produce a continuous solid-solution series from end-member CaSiO₃ past the hedenbergite composition, Ca_{0.5}Fe_{0.5}SiO₃, to the composition, expressed in terms of components wollastonite (Wo) and ferrosilite (Fs), corresponding to Wo₂₄Fs₇₆. The powder diffraction patterns for several compositions in this range were compared with those of wollastonite and bustamite, Ca_{0.5}Mn_{0.5}SiO₃, and claimed to be identical. The authors thus asserted that wollastonite could accept extensive Fe and Mn substitution for Ca without a change in the structure. More recently PEACOR and BUERGER (1962) determined the structure of bustamite and found it to be related but not equivalent to that of wollastonite. Powder diffraction patterns of the two phases, however, are almost indistinguishable.

In 1971, one of us (P.A.R.) determined the unit-cell parameters of a synthetic pyroxenoid of composition Wo₅₀Fs₅₀ (formed as the high-temperature transformation product of hedenbergite). Their similarity to those of bustamite suggested that this pyroxenoid represents the Fe analog of bustamite, or ferrobustamite, rather than "wollastonite solid solution" as postulated by BOWEN, SCHAIRER, and POSNJAK (1933). RUTSTEIN (1971) has published a study of the x-ray powder diffraction patterns of high-temperature pyroxenoid phases having compositions between Wo₁₀₀ and Wo₅₀Fs₅₀. He noted splitting of some major peaks between the compositions Wo₈₈Fs₁₂ and Wo₇₈Fs₂₂, and attributed this phenomenon to the appearance of a second phase. Analysis of the infra-red spectra of these pyroxenoids led to the claim that the Fe-rich phase is the iron analog of bustamite (RUTSTEIN and WHITE, 1971).

This paper presents single-crystal x-ray structure determinations of two pyroxenoids having compositions Wo₇₉Fs₂₁ and Wo₅₀Fs₅₀. The hypothesis of a bustamite-type structure for these compositions is confirmed. The Wo₅₀Fs₅₀ phase was further examined to compare its ferrobustamite structure with that of bustamite, Ca_{0.5}Mn_{0.5}SiO₃. The

Wo₇₉Fs₂₁ natural crystal was studied primarily to ascertain whether the ferrobustamite or the wollastonite structure is stable at significantly lower iron contents, and secondly to determine whether at such a composition the cation distribution would be ordered.

It is a pleasure to dedicate this work to Professor MARTIN J. BUERGER, from whom C.W.B. obtained so much inspiration and encouragement as a graduate student. Professor BUERGER's impact on silicate crystal chemistry is both significant and well-known. The structural studies on pyroxenoids carried on in his laboratory form much of the background for this study, and we want particularly to acknowledge our debt of gratitude for those many contributions.

Experimental procedure

Specimen description

The crystal of composition Wo₅₀Fs₅₀ was grown synthetically by VEBLEN (1969). According to his description, a starting mixture of 0.5053 g Fe, 1.2908 g Fe₂O₃, 1.5025 g SiO₂, and 2.9044 g CaSiO₃ was ground for three hours in an agate mortar. The mixture was then subjected to 1108°C and 2 kbar for 48 hours. The reaction product consisted almost entirely of a pyroxenoid phase, from which one crystal of sufficient size was found for single-crystal work.

The crystal of composition Wo₇₉Fs₂₁ was taken from a natural assemblage of pyroxenoid plus hedenbergite described by TILLEY (1948) as an ore skarn in dolomite invaded by the Beinn an Dubhaich granite at Skye, Scotland. The sample was kindly provided by Professor S. O. AGRELL of the University of Cambridge. An electron microprobe analysis was carried out on a crystal adjacent to that used for x-ray structure analysis, and is reported in Table 1. When Mg is ignored, Si assumed to be 2, and the cation numbers normalized to 2,

Table 1. *Electron microprobe analysis of Wo₇₉Fs₂₁ crystal from Skye, Scotland*

	Weight %	Cation numbers, based on 6 oxygen atoms
SiO ₂	53.30	2.079
FeO	10.44	0.341
MgO	0.06	0.003
MnO	1.58	0.052
CaO	34.63	1.477
	100.01	1.873

the formula becomes $\text{Ca}_{1.58}\text{Fe}_{0.38}\text{Mn}_{0.04}\text{Si}_2\text{O}_6$. This analysis is in substantial agreement with the wet chemical analysis reported by TILLEY (1948) that gave the formula $\text{Ca}_{1.65}\text{Fe}_{0.31}\text{Mn}_{0.04}\text{Si}_2\text{O}_6$. For purposes of structure analysis Fe and Mn have been combined because of their similar scattering factors to give a working formula corresponding to $\text{W}_{0.79}\text{F}_{8.21}$. The effects of chemical-analysis errors on the structural results for this material are deemed quite insignificant compared with possible errors due to twinning.

Space group and unit cell

Precession films of $\text{W}_{0.50}\text{F}_{8.50}$ resemble those of wollastonite, showing the same pseudomonoclinic symmetry. Using the same orientation of axes as reported for wollastonite, however, we find that all reflections with $k + l = \text{odd}$ are extinct. The space group is thus $A1$ or $A\bar{1}$. The unit-cell parameters as determined from the diffractometer orientation matrix were found to be close to those of bustamite (Table 2).

Table 2. *Unit-cell parameters*

	Wollastonite ¹	Bustamite ²	$\text{W}_{0.50}\text{F}_{8.50}$	$\text{W}_{0.79}\text{F}_{8.21}$ ³
a, Å	7.94	7.736	7.691	7.832
b, Å	7.32	7.157	7.112	7.229
c, Å	7.07	13.824	13.765	13.925
α	90° 2'	90° 31'	90° 22'	90° 1'
β	95° 22'	94° 35'	95° 19'	95° 24'
γ	103° 26'	103° 52'	103° 58'	103° 21'
Cell volume	397.8	740.4	727.2	763.5 Å ³

¹ PREWITT and BUERGER (1963).

² PEACOR and PREWITT (1963).

³ Obtained from diffraction pattern of twinned crystal.

The crystal of composition $\text{W}_{0.79}\text{F}_{8.21}$ was similarly aligned. On the basis of photographs of the $hk0$, $0kl$, and $1kl$ planes in reciprocal space, the space-group extinctions were judged to be the same as those found in the $\text{W}_{0.50}\text{F}_{8.50}$ diffraction patterns. Unit-cell parameters determined on the single-crystal diffractometer are listed in Table 2.

Data collection and refinement

Intensity data were measured on a Picker four-circle computer-controlled single-crystal diffractometer. Three reflections having high 2θ values were aligned accurately using a 1.4° take-off angle and

0.001 inch detector slits. The angular settings were used by the computer to calculate an orientation matrix (BUSING and LEVY, 1967) from which the cell parameters in Table 2 were derived. The integrated intensities of all non-extinct and non-equivalent reflections with 2θ less than 65° were then measured. These data were collected for both crystals using a take-off angle of 3.2° and $\text{MoK}\alpha$ radiation with a 0.002 inch thick $\text{Nb}\beta$ filter. Peaks were scanned with ω - 2θ scans at $1^\circ 2\theta$ per minute; background intensities were counted for 20 seconds on either side of the peaks. Standard reflections were measured periodically to verify alignment and x-ray intensity. The data were corrected for Lorentz and polarization effects, and for absorption by a numerical integration procedure (BURNHAM, 1966). Reflections whose integrated intensities were less than twice the standard deviation of I as calculated from counting statistics were considered unobserved and were not used in further structure analysis.

Structure refinements were carried out on an IBM 370 computer using RFINE, a full-matrix least-squares program written by L. W. FINGER. Scattering curves for fully ionized atoms were taken from CROMER and MANN (1968), and anomalous dispersion correction factors were those from the *International tables for x-ray crystallography* (Vol. III, page 215, 1962).

Atomic coordinates of bustamite relative to the $A\bar{1}$ cell (PEACOR and PREWITT, 1963) were used as a preliminary model for the $\text{W}_{0.50}\text{F}_{\text{S}50}$

Table 3. *Atom coordinates, temperature factors, and metal site occupancies*

Atom (multiplicity)	Bustamite ¹	$\text{W}_{0.50}\text{F}_{\text{S}50}$ ²	$\text{W}_{0.79}\text{F}_{\text{S}21}$ ³
M(1) (2)			
occupancy	1.0 Mn	0.23(1) Ca 0.77(1) Fe	1.00(4) Ca 0.00(4) Fe
x	0.2018	0.2067(2)	0.2000(8)
y	0.4284	0.4266(2)	0.4218(7)
z	0.3733	0.3731(1)	0.3776(4)
B	0.56	0.93(3)	0.71(10) \AA^2
M(2) (2)			
occupancy	1.0 Ca	0.78(1) Ca 0.22(1) Fe	0.82(4) Ca 0.18(4) Fe
x	0.1988	0.1989(2)	0.1994(8)
y	0.9411	0.9391(2)	0.9284(7)
z	0.3785	0.3759(1)	0.3755(4)
B	0.69	0.82(4)	1.05(10) \AA^2

Table 3. (Continued)

Atom (multiplicity)	Bustamite ¹	WO ₅₀ FS ₅₀ ²	WO ₇₉ FS ₂₁ ³
M(3) (1)			
occupancy	1.0 Mn	0.07 Ca 0.93 Fe	0.55 Ca ⁴ 0.45 Fe
<i>x</i>	1/2	1/2	1/2
<i>y</i>	1/4	1/4	1/4
<i>z</i>	1/4	1/4	1/4
<i>B</i>	0.56	0.72(4)	0.13(11) Å ²
M(4) (1)			
occupancy	1.0 Ca	0.92(2) Ca 0.08(2) Fe	0.55(6) Ca ⁴ 0.45(6) Fe
<i>x</i>	1/2	1/2	1/2
<i>y</i>	3/4	3/4	3/4
<i>z</i>	1/4	1/4	1/4
<i>B</i>	0.73	0.70(5)	1.47(16) Å ²
Si(1) (2)			
<i>x</i>	0.1768	0.1751(3)	0.1877(9)
<i>y</i>	0.3881	0.3904(3)	0.3980(9)
<i>z</i>	0.6343	0.6368(2)	0.6344(5)
<i>B</i>	0.34	0.65(3)	1.34(11) Å ²
Si(2) (2)			
<i>x</i>	0.1775	0.1775(3)	0.1902(10)
<i>y</i>	0.9434	0.9426(3)	0.9475(10)
<i>z</i>	0.6325	0.6312(2)	0.6346(5)
<i>B</i>	0.32	0.71(4)	1.53(12) Å ²
Si(3) (2)			
<i>x</i>	0.3950	0.3935(3)	0.3973(7)
<i>y</i>	0.7170	0.7179(3)	0.7244(7)
<i>z</i>	0.5218	0.5226(1)	0.5226(4)
<i>B</i>	0.16	0.62(3)	0.90(8) Å ²
O(1) (2)			
<i>x</i>	0.4316	0.4304(8)	0.425(3)
<i>y</i>	0.2400	0.2376(9)	0.233(3)
<i>z</i>	0.4027	0.4011(4)	0.403(1)
<i>B</i>	0.68	0.80(9)	2.1(4) Å ²
O(2) (2)			
<i>x</i>	0.4036	0.4021(7)	0.414(2)
<i>y</i>	0.7178	0.7096(8)	0.727(2)
<i>z</i>	0.4069	0.4068(4)	0.410(1)
<i>B</i>	0.57	1.18(11)	1.1(3) Å ²
O(3) (2)			
<i>x</i>	0.3126	0.3141(8)	0.318(2)
<i>y</i>	0.4725	0.4724(9)	0.471(2)
<i>z</i>	0.7293	0.7312(4)	0.731(1)
<i>B</i>	0.48	1.18(10)	1.4(3) Å ²

Table 3. (Continued)

Atom (multiplicity)	Bustamite ¹	Wo ₅₀ Fs ₅₀ ²	Wo ₇₉ Fs ₂₁ ³
O(4) (2)	<i>x</i>	0.3017	0.3032(8)
	<i>y</i>	0.9303	0.9279(9)
	<i>z</i>	0.7315	0.7303(4)
	<i>B</i>	0.48	1.00(10)
O(5) (2)	<i>x</i>	0.0261	0.0276(8)
	<i>y</i>	0.6167	0.6155(9)
	<i>z</i>	0.3549	0.3510(4)
	<i>B</i>	0.64	1.56(13)
O(6) (2)	<i>x</i>	0.0280	0.0295(9)
	<i>y</i>	0.1627	0.1638(10)
	<i>z</i>	0.3717	0.3744(5)
	<i>B</i>	0.66	1.76(13)
O(7) (2)	<i>x</i>	0.2574	0.2540(7)
	<i>y</i>	0.5047	0.5108(8)
	<i>z</i>	0.5393	0.5424(4)
	<i>B</i>	0.57	1.05(9)
O(8) (2)	<i>x</i>	0.2728	0.2740(10)
	<i>y</i>	0.8739	0.8800(9)
	<i>z</i>	0.5411	0.5388(4)
	<i>B</i>	0.29	1.01(9)
O(9) (2)	<i>x</i>	0.1852	0.1866(10)
	<i>y</i>	0.1676	0.1703(9)
	<i>z</i>	0.6147	0.6176(4)
	<i>B</i>	1.34	2.15(12)

¹ From PEACOR and BUERGER (1962). Coordinates for their $P\bar{1}$ cell have been transformed to those for the $A\bar{1}$ cell used here.

² Temperature factors correspond to equivalent isotropic B 's calculated from the anisotropic temperature factor tensor according to $B_{\text{equiv}} = \frac{4}{3} \sum_i \sum_j \beta_i \mathbf{a}_i \cdot \mathbf{a}_j$ (HAMILTON, 1959). Standard deviations in parentheses represent uncertainty in the least significant figures, *i.e.* for 0.2067(2) read 0.2067 \pm 0.0002. The occupancy of M(3) was a dependent parameter obeying the bulk chemical constraint.

³ Coordinates listed are those from refinement using all reflections. Temperature factors are from isotropic refinement. Standard deviations are given as for Wo₅₀Fs₅₀ (see footnote ²).

⁴ Refined occupancy values for M(3) and M(4) in Wo₇₉Fs₂₁ are almost certainly incorrect. See text for discussion.

structure. This model is ordered, with Ca and Fe each filling one general position and one special position¹. Refinement for five cycles varied one scale factor, the atom parameters, and isotropic temperature factors. At this stage temperature factors of the sites assigned as Ca were low and those for the sites containing Fe were high. This was a clear indication that the assumed cation distribution was incorrect, so in the next three least-squares the occupancies of the metal sites were varied in addition to the other parameters. Occupancy variation was carried out using the procedure designed by FINGER (1969) in which total cation content was constrained to agree with the chemical composition. The result corresponded essentially to a reversal of Ca and Fe among the four sites, and further analysis led to the discovery of a labeling error arising from errors in the atomic coordinates of the original model (see footnote 1). The parameters were further refined for four additional cycles, after which convergence was reached at a weighted R value of 5.60%. Anisotropic temperature factors were substituted and after two additional cycles of refinement convergence was attained with $R_w = 4.40\%$ and $R = 6.20\%$. Details of the structure are given in Tables 3 and 4. Bond distances and angles were computed using the program BADTEA (L. W. FINGER); the standard errors contain contributions from errors in the refined atom coordinates only.

Since the $hk0$, $0kl$, and $1kl$ precession photographs of the natural crystal of composition $\text{Wo}_{79}\text{Fs}_{21}$ were essentially identical to the corresponding photographs of the synthetic $\text{Wo}_{50}\text{Fs}_{50}$ crystal, except for an apparently larger mosaic spread, the parameters derived from refinement of the latter crystal were used as a preliminary model in refinement of the former. The Mn found in the analysis was combined with Fe and the total assigned to the scattering curve for Fe^{2+} . In the first three cycles of least-squares one scale factor, atom parameters, isotropic temperature factors, and metal site occupancies were varied, and the R_w value was reduced to 8.80%. Two more cycles were run varying

¹ The coordinates listed in Table 2 of PEACOR and PREWITT (1963) for the three Si atoms, O(3), O(4), O(8), and O(9) correspond to a shift of $b/2$ relative to the positions given in the original structure determination of bustamite by PEACOR and BUERGER (1962). Due to the pseudosymmetry of the unit cell, this shift of certain coordinates is roughly equivalent to a relabeling of sites. The labeling and coordinates given for bustamite in this paper (Table 3) correspond to those of PEACOR and BUERGER (1962) transformed to the $A\bar{1}$ cell.

² Weighted $R = R_w = [\sum w(F_{\text{obs}} - F_{\text{calc}})^2 / \sum w(F_{\text{obs}})^2]^{1/2}$; Unweighted $R = R = \sum |F_{\text{obs}}| - |F_{\text{calc}}| / \sum |F_{\text{obs}}|$.

Table 4. *Interatomic distances*

Atom pair	Bustamite ¹	WO ₅₀ FS ₅₀ ²	WO ₇₅ FS ₂₁ ³
M(1)—O(1)	2.499(6) Å	2.432(6) Å	2.475 Å
O(2)	2.286	2.218(6)	2.426
O(4)	2.163	2.164(6)	2.336
O(5)	2.144	2.149(6)	2.302
O(6)	2.041	2.031(7)	2.271
O(7)	2.335	2.375(5)	2.359
Mean of 6	2.245	2.228	2.362
M(2)—O(1)	2.437	2.418(6)	2.510
O(2)	2.531	2.531(6)	2.450
O(3)	2.298	2.245(6)	2.296
O(5)	2.382	2.365(6)	2.310
O(6)	2.302	2.292(7)	2.280
O(8)	2.358	2.330(5)	2.372
O(9)	2.899	2.889(7)	—
Mean of 6	2.384	2.364	2.370
Mean of 7	2.457	2.439	—
M(3)—O(1) (× 2)	2.215	2.192(5)	2.244
O(3) (× 2)	2.154	2.138(6)	2.173
O(4) (× 2)	2.241	2.195(6)	2.230
Mean of 6	2.203	2.175	2.216
M(4)—O(2) (× 2)	2.344	2.348(5)	2.396
O(3) (× 2)	2.412	2.375(6)	2.383
O(1) (× 2)	2.421	2.420(6)	2.417
O(9) (× 2)	2.891	2.827(7)	2.677
Mean of 6	2.392	2.381	2.399
Mean of 8	2.517	2.493	2.466
Si(1)—O(3)	1.628	1.613(7)	1.623
O(5)	1.587	1.574(6)	1.577
O(7)	1.645	1.643(5)	1.625
O(9)	1.616	1.613(6)	1.643
Mean	1.619	1.611	1.617
Si(2)—O(4)	1.626	1.617(6)	1.534
O(6)	1.585	1.583(7)	1.549
O(8)	1.647	1.641(6)	1.637
O(9)	1.613	1.618(6)	1.659
Mean	1.618	1.615	1.595

Table 4. (*Continued*)

Atom pair	Bustamite ¹	W ₀₅₀ Fs ₅₀ ²	W ₀₇₉ Fs ₂₁ ³
Si(3)—O(1)	1.600	1.601(6)	1.607
O(2)	1.595	1.603(6)	1.590
O(7)	1.660	1.640(5)	1.681
O(8)	1.671	1.665(6)	1.677
Mean	1.632	1.627	1.638

¹ From PEACOR and PREWITT (1963).

² Standard deviations in parentheses represent uncertainty in the least significant figures, *i.e.* for 2.432(6) read 2.432 ± 0.006 . Errors do not include the effects of errors in cell parameters.

³ Distances for W₀₇₉Fs₂₁ are only approximate due to twinning (see text), thus no standard deviations are listed. The precision is probably no greater than about ± 0.03 to 0.05 \AA .

the same parameters, but the R value remained unchanged. During these two cycles, however, the temperature factor of the M(3) site decreased to the anomalously low value of 0.13, while that of the M(4) site increased to 1.47. The occupancy parameters indicated that the general positions, M(1) and M(2), were filled almost entirely with Ca and that the special positions, M(3) and M(4), were filled with approximately equal amounts of Fe and Ca. Yet the anomalous temperature factors for M(3) and M(4), along with the high R value, suggested that Fe and Ca were, in fact, more ordered in M(3) and M(4). Bond distances within the metal coordination polyhedra substantiated this; the average M(3)—O distance was 2.21 \AA , consistent with a site filled mainly by Fe, and the average M(4)—O distance was 2.40 \AA , consistent with a site filled primarily with Ca.

In view of these indications of ordering, the model was changed accordingly and another cycle of least-squares was carried out using unit weights for all F_{obs} . The model refined back to a disordered occupancy with anomalous temperature factors for the M(3) and M(4) sites. A cycle was run without chemical constraints but this yielded the meaningless result of a negative amount of Fe. A further cycle was run using anisotropic temperature factors since disordering of cations can result in very elongated apparent ellipsoids of vibration. However, this cycle failed to reduce the R value, and the temperature-factor tensor for one oxygen atom was not positive-definite. A Fourier difference map calculated at this stage failed to show any interpretable features. Thus it seemed at this point that the data must be in error.

Although optical examination of this crystal had shown uniform extinction under crossed nicols, the possibility of twinning was then further explored. Study of typical twinning in the similar wollastonite structure (PREWITT and BUERGER, 1963) had shown that twins with (100) as the twin plane could be detected only on odd-level c -axis and odd-level b -axis precession photographs. Since only $hk0$, $0kl$, and $1kl$ precession photographs of this crystal had been examined, similar twinning would not have been detected. An odd-level c -axis precession photograph taken at this time did reveal that the crystal was composed of approximately equal volumes of two twins having (100) as their composition plane.

From consideration of twinning relations (see below) it was clear that all reflections with $k = \textit{even}$ correspond to the superposition of reflections from the two twin components. The $k = \textit{odd}$ reflections, however, contain contributions from only one of the twins. An attempt was therefore made to refine the model using only the $k = \textit{odd}$ reflections, which, because of the pseudosymmetry of the structure, are systematically weak. Because only 369 observed $k = \textit{odd}$ reflections were available, a model with fixed occupancies and temperature factors was prepared. The occupancies of the M(1) and M(2) sites were fixed at values obtained from the previous cycle, but all remaining Fe was placed in M(3), giving it 90% Fe. Temperature factors were taken from the last isotropic temperature factor cycle of the $\text{Wo}_{50}\text{Fe}_{50}$ refinement. Several cycles of least-squares were carried out with this model varying only atomic coordinates. The weighted R value converged at 19.6%.

From least-squares analysis using only the $k = \textit{odd}$ reflections and from the previous refinement using all reflections we believe enough information is available to deduce a substantially correct structure. Further discussion of the validity of this deduction is presented later. The parameters presented in Table 3 (atomic coordinates) and Table 4 (interatomic distances) are from refinements with all observed reflections. The interatomic distances should be considered only approximate because of the twinning problem.

The ferrobustamite structures

The ferrobustamite structure is close to that of bustamite, which has already been thoroughly described elsewhere (PEACOR and BUERGER, 1962), and compared with that of wollastonite (PEACOR and PREWITT, 1963). Basically ferrobustamite is a pyroxenoid having

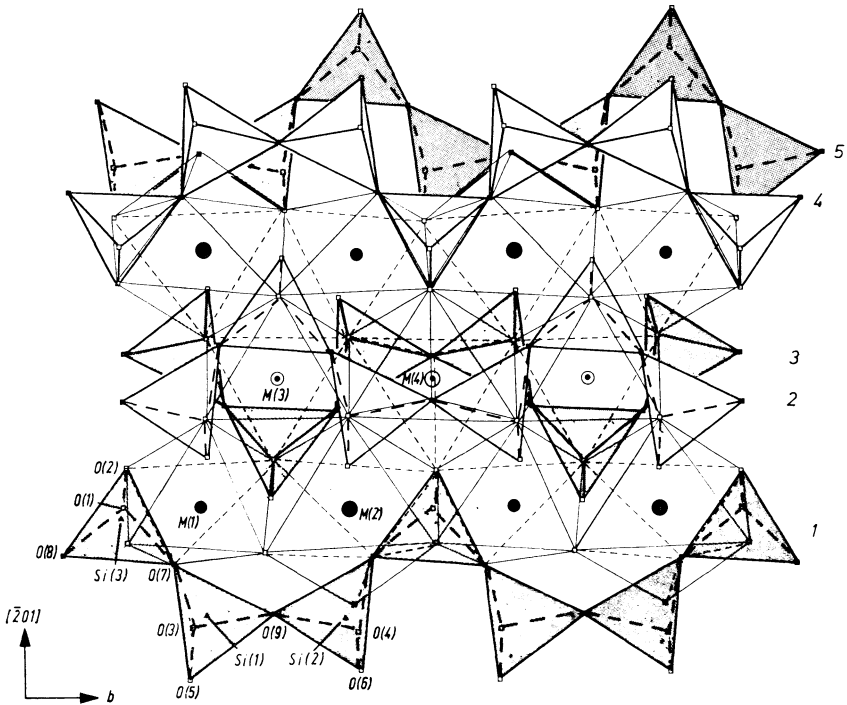


Fig. 1. Projection of the ferrobustamite structure of composition $Wo_{50}Fs_{50}$ onto the plane (102), parallel to the layers of silicate chains and bands of metal polyhedra. Silicate tetrahedral chains below the octahedral band are shaded; those above unshaded. Numbers on right correspond to chain numbers used in text and are for identification only. M(3) and M(4) lie on inversion centers

single silicate chains with repeat lengths of three tetrahedra-*Dreierketten*. In the $A\bar{1}$ cell used here, there are four equivalent silicate chains per unit cell. The structure contains four crystallographically distinct metal sites; two occupy general positions and two are in special positions on inversion centers. The metal sites are arranged parallel to the silicate chains in three coplanar infinite chains of coordination polyhedra that share edges to make up a band.

As seen in Fig. 1 silicate chains 2 and 3 are centrosymmetrically related with apices of their tetrahedra pointing toward each other. The inversion centers relating these two chains are the locations of cation sites M(3) and M(4). The M(3) site has fairly regular octahedral coordination, but the M(4) site has six near neighbors in regular octahedral coordination plus two additional far neighbors, the O(9) atoms linking adjacent silicate chains, that may be considered part

of its coordination polyhedron. These sites are thus roughly analogous to the M(1) sites of pyroxenes. The two chains of metal polyhedra, M(1) and M(2), in the general positions each link four silicate chains. The M(1) and M(2) coordination polyhedra are similarly distorted octahedra, except that the M(2) site may have additional distant coordination with one oxygen, the chain-linking O(9) atom. These two metal polyhedra serve approximately the same bridging function as the M(2) polyhedra of pyroxenes.

Pseudomonoclinic substructure

Within the bustamite triclinic cell there is a prominent pseudomonoclinic substructure with symmetry $A2/m$ having the same volume as the triclinic cell. Pseudomirror planes perpendicular to the b axis can be passed through O(9) and through O(1), O(2), and Si(3). These then make O(3) pseudoequivalent to O(4), O(5) to O(6), O(7) to O(8), and Si(1) to Si(2). In the various bustamite structures examined these equivalences hold to within 0.03 in fractional coordinates. The two cations, M(3) and M(4), occupy special positions at the intersections of diad axes and the pseudomirror planes, and the two general-position cation sites, M(1) and M(2), are pseudoequivalent by virtue of the pseudomirror planes. The deviation from monoclinic symmetry is such that M(2) has a larger coordination polyhedron than M(1), and may have an additional bond with O(9). The polyhedra coordinating metal sites in special positions are also of different sizes; the M(4) polyhedron is larger than that of M(3), and M(4) bonds additionally to O(9) without violating the pseudosymmetry.

Pseudotranslational symmetry also exists between certain atoms. To a first approximation, the atoms lying off the pseudomirror planes of the subcell have pseudomonoclinic equivalents separated by $b/2$. These atoms, therefore, make essentially no contribution to the scattered intensity for reflections with $k = \text{odd}$. Since the inversion centers occupied by M(3) and M(4) are separated by exactly $b/2$, the only contribution from these atoms to the $k = \text{odd}$ reflections arises from differences in scattering power and thermal vibrations. The $k = \text{odd}$ reflections, are therefore, significantly weaker than those with $k = \text{even}$, to whose scattered intensity all atoms contribute.

The triclinic cell of normal, or $1T$, bustamite can be regarded as the result of stacking pseudomonoclinic subcells along the a axis with a $b/4$ offset between cells (see Fig. 8b, PREWITT and BUERGER, 1963). The pseudomonoclinic subcell and the triclinic cell thus have their

b and c axes coincident, but their a axes differ in direction. The symmetry operations of the pseudomonoclinic unit are offset at the cell boundaries, thus at the level of several unit cells there are no symmetry elements other than inversion centers. The space group of $1T$ bustamite is thus $A\bar{1}$.

If, however, the $b/4$ offset in the stacking sequence along a were reversed every unit cell (see Fig. 8c, PREWITT and BUERGER, 1963), a double monoclinic cell containing two subcells would be created. An a glide perpendicular to b at $y = 1/2$ would relate atoms in one subcell to their pseudoequivalents in the next subcell, *e.g.* O(3) to O(4), O(5) to O(6), etc. For the double cell to have true monoclinic symmetry the subcell must have true $A2/m$ symmetry. If such were the case, the double cell would have space group $A2/a$ and in standard stacking nomenclature the structure would be termed a $2M$ bustamite.

Although a monoclinic $2M$ bustamite has never been reported, the equivalent $2M$ wollastonite, known as parawollastonite, does exist and its structure has been refined in space group $P2_1/a$ (TROJER, 1967). Other stacking polymorphs of wollastonite have been reported (WENK, 1969), including disordered structures that apparently correspond to random variation in the direction of the $b/4$ offset between subcells. Bustamite differs from wollastonite primarily in the arrangement of silicate chains relative to the bands of metal coordination polyhedra (PEACOR and PREWITT, 1963). This difference accounts for the A centering of the bustamite lattice in contrast to the primitive wollastonite lattice, and is thought to be caused (PREWITT and PEACOR, 1964) by the ordering of Mn or Fe into M(3) and Ca into M(4) in the bustamite arrangement, as opposed to the equivalence of these two sites in a general position in wollastonite. PREWITT and PEACOR (1964) have suggested that a geometrical consequence of these differences is the unlikelihood of forming the $2M$ stacking sequence with bustamite units because of distortions within the octahedral bands that would be required to achieve proper fit.

Just one reversal of the $b/4$ offset in the stacking sequence along a would correspond to a stacking fault and would lead to a twinned crystal (see Fig. 8a, PREWITT and BUERGER, 1963). Polysynthetic twins would result from several irregularly spaced reversals. This mechanism does take place in bustamite, and accounts for the twinning observed in our crystal of $W_{0.79}F_{S_{21}}$. The effects of such twinning on diffraction patterns and on our structure analysis of $W_{0.79}F_{S_{21}}$ are discussed below.

$W_{0.5}F_{5.0}$ coordination polyhedra

Variations in the bustamite structure are best described in terms of the configurations and sizes of the metal coordination polyhedra, which reflect the departures from exact monoclinic symmetry of the substructure. Also important is the position of O(9), which is determined by the kink of the silicate chain. O(9) can approach the M(2) and M(4) sites sufficiently to coordinate loosely, and this further distinguishes these sites from M(1) and M(3). These factors permit the general structure to conform to the requirements of different cation substitutions.

The structure of the crystal of $W_{0.5}F_{5.0}$ is essentially identical with the bustamite structure of $Ca_{0.5}Mn_{0.5}SiO_3$ refined by PEACOR and BUEGER (1962). The single silicate tetrahedral chain departs somewhat from monoclinic symmetry, and thus the substructure has only pseudomonoclinic symmetry. The M(2) polyhedron is larger than the M(1) polyhedron (Table 4, Fig.1), and O(9) is sufficiently close to be considered as coordinated to M(2) [M(2)—O(9) = 2.89 Å]. In view of these facts, the larger 7-coordinated M(2) site accommodates mainly Ca, whereas the smaller 6-coordinated M(1) site accommodates mainly Fe. The special positions containing M(3) and M(4) are similarly ordered. M(4) is larger than M(3), and two O(9) atoms are close enough to coordinate loosely with it [M(4)—O(9) = 2.82 Å]. Therefore Ca occupies M(4) with its irregular 8-coordination whereas Fe occupies the smaller regular octahedral M(3) site. The size difference between M(3) and M(4) polyhedra, in special positions, is greater than that between M(1) and M(2) polyhedra in general positions. This is reflected in greater ordering among the special positions as compared to the general positions (Table 3).

Variations in the Si—O bond distances can be explained in terms of valence saturation and classical bond strengths. The chain-linking oxygen atoms, O(7), O(8), and O(9), have their classical valence satisfied by the two Si—O bonds. O(7) and O(8) are, in addition, coordinated to one Ca each, and thus are oversaturated with bonds adding up to $2\frac{1}{2}$. The Si—O(7) and Si—O(8) bonds are consequently weaker and longer (1.65 Å) than the other Si—O bonds. O(9) is coordinated to two Ca atoms in addition to the two Si atoms, but both Ca—O(9) distances are very long, so that these do not contribute significantly to oversaturation. The Si—O(9) distances (1.651 Å) are therefore nearly the same as those to O(3) and O(4), which are exactly saturated

with bonds to one Si and three metal atoms each. O(1) and O(2) are also saturated with bonds to one Si and three metal atoms, but these Si—O distances are slightly smaller (1.605 Å) because Si(3), to which O(1) and O(2) are coordinated, is also coordinated to the oversaturated oxygen atoms, O(7) and O(8). O(5) and O(6) are undersaturated with bonds to one Si and only two metal atoms each, and thus have the shortest Si—O distances (1.58 Å).

W₀₇₉Fs₂₁ structure and twinning

Twinning of the type encountered in our crystal of W₀₇₉Fs₂₁ is due to one or several reversals of the $b/4$ offset between subcells in the stacking sequence along the a axis. The twinning is not optically apparent, and, as stated previously, its effects on the diffraction pattern are only visible on odd-level b - or c -axis photographs. Because of the geometry and pseudosymmetry of the subcells, reciprocal lattice planes normal to b with $k = \text{even}$ from one twin component superimpose on corresponding reciprocal lattice planes with $k = \text{even}$ from the other twin component, in a manner similar to that described for wollastonite and pectolite by PREWITT and BUERGER (Fig. 9, 1963). The superimposition will not be exact unless the subcells are perfectly monoclinic. The $k = \text{odd}$ reflections from the two twin components do not superimpose, therefore a twinned crystal will give a diffraction pattern with two sets of k odd reflections and only one superimposed set of k even reflections.

Focusing attention on the k even reflections, the $h'k'l'$ reflection from twin component 2 that superimposes on hkl from component 1 will be the latter's pseudomonoclinic equivalent, since the twin operation can be thought of as a twofold rotation around b with (100) as the composition plane. If the subcell had perfect monoclinic symmetry and if the volumes of the two twin components were equal, the intensities of the superimposed reflections would be exactly twice those diffracted from a single component.

Refinement of the W₀₅₀Fs₅₀ structure showed that its substructure is close to monoclinic. Since the intensity distribution in W₀₇₉Fs₂₁ is very nearly the same as in W₀₅₀Fs₅₀ and since the two twin components are estimated to have close to equal volumes, the use of k even superimposed reflections in refinement, properly scaled to the k odd data, should yield a reasonably good approximation to the correct structure. The parameters for W₀₇₉Fs₂₁ listed in Table 3 are those resulting from this procedure.

Compared with the M(1) and M(2) sites in $\text{Wo}_{50}\text{Fs}_{50}$, the general-position M(2) site has lost its loose bond with O(9), and the M(1) polyhedron has grown in size. The two sites are thus practically identical in occupancy, primarily Ca, and have polyhedra that are very similar in size and shape. This is consistent with monoclinic symmetry of the substructure. The M(3) and M(4) sites, in special positions, are not related by pseudosymmetry and have different-sized coordination polyhedra. The M(4) site is, as in the $\text{Wo}_{50}\text{Fs}_{50}$ structure, coordinated to two O(9) atoms in addition to its six near neighbors, but the M(4) to O(9) bonds are shorter in the $\text{Wo}_{79}\text{Fs}_{21}$ structure. On the basis of bond distances (Table 4) it appears that M(3) is primarily occupied by Fe while M(4) contains mainly Ca, similar to the distribution in $\text{Wo}_{50}\text{Fs}_{50}$.

The occupancy parameters for M(3) and M(4) (Table 3) disagree with conclusions drawn from bond distances. Furthermore the thermal parameters for these sites are clearly erroneous when compared with those for the same sites in $\text{Wo}_{50}\text{Fs}_{50}$ and bustamite, or, for that matter, with any metal site in similar silicate structures. If, however, the true occupancies of M(3) and M(4) are close to those consistent with bond distances, namely Fe in M(3) and Ca in M(4), then the temperature factors represent compensation by the refinement process for incorrectly converged occupancy values. Since M(3) and M(4) lie on inversion centers separated by $b/2$, direct determination of differing occupancies depends heavily on availability of precise *k odd* data. But these reflections are uniformly weak for reasons stated previously, and this fact combined with the likely errors in *k even* data due to twinning undoubtedly explains why the least-squares procedure has yielded erroneous occupancy parameters.

Abnormally high thermal parameters for the silicon and oxygen atoms also appear to result from twinning and lack of strict validity of our assumptions regarding the *k even* data. Departures of the real substructure from monoclinic symmetry and the twin components from equal volumes will have introduced unpredictable averaging effects that show up most readily in thermal parameters, but also appear to have influenced atom positions to some extent, particularly those making up the Si(2) tetrahedron.

The results from refinement of atom coordinates using the limited and weak *k odd* reflections that are unaffected by twinning, although no more reliable because of the high *R* value, do confirm the sizes and shapes of metal coordination polyhedra. Similar to the results using all data, M(1) and M(2) are both large 6-coordinated sites with mean

M—O = 2.35 Å containing mostly Ca. M(3) is a small, fairly regular octahedral site with mean M(3)—O = 2.21 Å containing primarily Fe, and M(4) has 8-coordination with mean M(4)—O = 2.42 Å and thus contains mainly Ca. In spite of bond-distance errors estimated to be as high as ± 0.05 Å, the conclusion that Fe is concentrated primarily in M(3) seems substantiated.

Discussion

Structure determinations of pyroxenoids having compositions $\text{Wo}_{50}\text{Fs}_{50}$ (synthetic) and $\text{Wo}_{79}\text{Fs}_{21}$ (natural) confirm the existence of a Ca-Fe pyroxenoid mineral analogous to bustamite. We propose accordingly that this mineral be called ferrobustamite. From the crystal-structure relations between wollastonite and ferrobustamite it is clear the two phases are different. Transformation of one structure to the other requires at the very least a shift of half the silicate chains by $b/2$ relative to the others. The distribution of metal cations in the two phases at compositions near their coexistence must also be different. Because the M(3) and M(4) sites of ferrobustamite transform to one general-position site, Ca(3), in wollastonite, the ordering scheme for Fe in $\text{Wo}_{79}\text{Fs}_{21}$ is impossible in the wollastonite structure. RUTSTEIN (1971) has suggested that the 12% Fe that wollastonite can accept in solid solution is probably disordered over the Ca(1) and Ca(2) sites, which are roughly equivalent to M(1) and M(2) in ferrobustamite, but this has not been confirmed by any structural study.

The fact that ferrobustamite appears not to be the stable pyroxenoid phase for compositions less Fe rich than approximately $\text{Wo}_{80}\text{Fs}_{20}$ can be explained by examining its structure. Over the composition range examined, the M(2) and M(4) polyhedra seem to be sufficiently large to accept mainly Ca. As the composition changes from $\text{Wo}_{50}\text{Fs}_{50}$ toward $\text{Wo}_{79}\text{Fs}_{21}$ the M(1) polyhedron expands to accommodate the additional Ca. The M(3) polyhedron, on the other hand, seems structurally constrained, probably by the geometrical requirements of the silicate chains, to a size that excludes large amounts of Ca. Thus the composition change appears to be accomplished primarily by Ca substitution for Fe in M(1). At the point where Ca completely fills M(1), M(2), and M(4), and Fe remains exclusively in M(3), the composition will be $\text{Wo}_{5/6}\text{Fs}_{1/6}$. This matches rather closely the lower limit for Fe content reported by RUTSTEIN (1971) on the basis of powder diffraction studies.

The two-pyroxenoid phase diagram proposed by RUTSTEIN (Fig. 6, 1971) for the CaSiO_3 — $\text{CaFeSi}_2\text{O}_6$ join helps explain the paucity of natural occurrences of Ca-Fe pyroxenoids with high Fe contents. His diagram indicates that the only phase capable of accepting more than about 12% Fe is ferrobustamite and that it is stable only at temperatures above about 800°C (at 1 kbar $P_{\text{H}_2\text{O}}$ and f_{O_2} defined by the quartz-fayalite-magnetite buffer). These temperatures will be reached only in contact-metamorphic skarn zones, and this is indeed the type of locality in which the one reported pyroxenoid with such a high Fe content is found (TILLEY, 1948). On the other hand, pyroxenoids with wollastonite structures containing less than 12% Fe are stable at lower temperatures, and such occurrences are more common (TILLEY, 1937).

The limits of solid solution of Fe and Mn in wollastonite have been set at approximately 12 atom % and 25 atom % respectively on the basis of spectral studies (RUTSTEIN and WHITE, 1971). Above these concentrations the bustamite structure becomes the stable pyroxenoid phase. The behavior of Mg in wollastonite, on the other hand, is not as well characterized. Analyses of natural phases rarely report more than 3% Mg in wollastonites (DEER, HOWIE, and ZUSSMAN, 1967). FERGUSON and MERWIN (1919) reported a high-temperature synthetic metasilicate phase extending from CaSiO_3 to 16% MgSiO_3 , but the structural details are unknown. Whether a bustamite-type pyroxenoid exists at higher Mg concentrations is not clear. A search for magnesian-bustamite and examination of the solid solution relations between Mg, Fe, and Mn bustamites now deserve attention in further studies of *Dreierketten* pyroxenoids.

Acknowledgments

We thank Dr. S. O. AGRELL of the University of Cambridge for kindly providing the natural ferrobustamite crystals used in this study. Dr. JOSEPH R. SMYTH helped with many computing problems, and Mr. PETER LYTTLE kindly performed the electron microprobe analysis. This research was supported by National Science Foundation grant GA-12852.

References

- N. L. BOWEN, J. F. SCHAIRER, and E. POSNJAK (1933), The system CaO — FeO — SiO_2 . *Amer. J. Sci.* **26**, 193—284.
C. W. BURNHAM (1966), Computation of absorption corrections, and the significance of end effect. *Amer. Mineral.* **51**, 159—167.

- W. R. BUSING and H. A. LEVY (1967), Angle calculations for 3- and 4-circle x-ray and neutron diffractometers. *Acta Crystallogr.* **22**, 457–464.
- D. T. CROMER and J. B. MANN (1968), X-ray scattering factors computed from numerical Hartree-Fock wave functions. *Acta Crystallogr. A* **24**, 321–324.
- W. A. DEER, R. A. HOWIE, and J. ZUSSMAN (1967), *Rock forming minerals*, Vol. 2, Longmans, Green, and Co. Ltd., London.
- J. B. FERGUSON and H. MERWIN (1919), Wollastonite and related solid solutions in the ternary system lime—magnesia—silica. *Amer. J. Sci.*, [4] **48**, 165–189.
- L. W. FINGER (1969), Determination of cation distributions by least-squares refinement of single-crystal x-ray data. *Carnegie Inst. Wash. Yearbook* **67**, 216–217.
- W. C. HAMILTON (1959), On the isotropic temperature factor equivalent to a given anisotropic temperature factor. *Acta Crystallogr.* **12**, 609–610.
- D. R. PEACOR and M. J. BUERGER (1962), Determination and refinement of the crystal structure of bustamite, $\text{CaMnSi}_2\text{O}_6$. *Z. Kristallogr.* **117**, 331–343.
- D. R. PEACOR and C. T. PREWITT (1963), Comparison of the crystal structures of wollastonite and bustamite. *Amer. Mineral.* **48**, 588–596.
- C. T. PREWITT and M. J. BUERGER (1963), Comparison of the crystal structures of wollastonite and pectolite. *Mineral. Soc. Amer. Spec. Pap.* **1**, 293–302.
- C. T. PREWITT and D. R. PEACOR (1964), Crystal chemistry of pyroxenes and pyroxenoids. *Amer. Mineral.* **49**, 1527–1542.
- M. S. RUTSTEIN (1971), Reexamination of the wollastonite-hedenbergite equilibrium. *Amer. Mineral.* **56**, 2040–2052.
- M. S. RUTSTEIN and W. B. WHITE (1971), Vibrational spectra of high calcium pyroxenes and pyroxenoids. *Amer. Mineral.* **56**, 877–887.
- C. E. TILLEY (1937), Wollastonite solid solutions from Sawt Hill. *Mineral. Mag.* **24**, 569–572.
- C. E. TILLEY (1948), On iron-wollastonites in contact skarns: An example from Skye. *Amer. Mineral.* **33**, 736–738.
- F. J. TROJER (1967), Crystal structure of parawollastonite. *Naturwiss.* **54**, 536.
- D. R. VEBLEN (1969), Crystal structures of hedenbergite and ferrosalite, A. B. Thesis, Harvard Univ.
- H. R. WENK (1969), Polymorphism of wollastonite. *Contrib. Mineral. Petrol.* **22**, 238–247.